

# Bragg-Bose glass phase in vortex states of high- $T_c$ superconductors with sparse and weak columnar defects

Yoshihiko Nonomura\* and Xiao Hu

Computational Materials Science Center, National Institute for Materials Science, Tsukuba, Ibaraki 305-0047, Japan

(Dated: October 31, 2018)

Phase diagram of vortex states of high- $T_c$  superconductors with *sparse and weak* columnar defects is obtained by large-scale Monte Carlo simulations of the three-dimensional anisotropic, frustrated XY model. The Bragg-Bose glass phase characterized by hexagonal Bragg spots and the diverging tilt modulus is observed numerically for the first time at low density of columnar defects. As the density of defects increases, the melting temperature increases owing to “selected pinning” of flux lines. When the density of defects further increases, the transition to the Bose glass phase occurs. The interstitial liquid region is observed between these two glass phases and the vortex liquid phase.

PACS numbers: 74.25.Qt, 74.62.Dh, 74.25.Dw

In vortex states of high- $T_c$  superconductors, columnar defects introduced by heavy-ion irradiation are strong pinning centers of flux lines, and dramatically enhance the critical current. [1] Nelson and Vinokur [2] analyzed these defects and derived a phase transition between the Bose glass (BG) and vortex liquid (VL) phases. They also showed that this system can be mapped to two-dimensional interacting bosons in a random potential and that this phase transition corresponds to a localization transition of interacting bosons. In the case of dense and strong columnar defects, every flux line is trapped by randomly-distributed columnar defects at low temperatures, and the BG phase naturally appears. Many numerical studies [3, 4, 5] have been made in this case.

In the case of sparse and strong columnar defects, part of flux lines are not trapped by defects, and physical properties are more complicated. At low temperatures untrapped flux lines are also frozen owing to interactions with trapped flux lines, and the BG phase is stable. At intermediate temperatures the defects still trap some flux lines but other interstitial ones are freely moving around, and the resistivity becomes finite. This region is called as the interstitial liquid (IL). [6] At high temperatures all flux lines are depinned and the VL phase appears. It is not clarified yet whether there exists a phase transition or merely a crossover between the IL and VL. A numerical simulation was attempted [7] in this case, and the existence of the BG phase was confirmed. Two kinds of BG phases for dense or sparse columnar defects are divided by the Mott insulator phase at the matching field. Recently the transition between these two (strong and weak) BG phases was observed numerically. [8]

In pure systems, the triangular flux-line lattice (FLL) is formed below the melting temperature  $T_m$ . Is such order completely destroyed by introducing infinitesimal columnar defects? In vortex states with point defects, the long-range order of vortex positions is destroyed by

infinitesimal defects, but the Bragg glass phase [9, 10, 11] characterized by the *quasi long-range order* of vortex positions and Bragg spots of the structure factor is stable up to a considerable density of point defects. In the present Letter, we numerically show that a similar phase with Bragg spots associated with hexagonal symmetry is also observed in the case of *sparse and weak* columnar defects. Since the tilt modulus shows a diverging behavior in this phase, it corresponds to the Bragg-Bose glass (BBG) phase. [11] When the density of columnar defects increases, a phase transition to the BG phase takes place. We also find that the IL region exists above the BBG or BG phases. These results are summarized in Fig. 1.

In this study we perform large-scale Monte Carlo simulations based on the three-dimensional anisotropic, frustrated XY model on a simple cubic lattice [12, 13]:

$$\mathcal{H} = - \sum_{i,j \in ab \text{ plane}} J_{ij} \cos(\phi_i - \phi_j - A_{ij}) - \frac{J}{\Gamma^2} \sum_{m,n \parallel c \text{ axis}} \cos(\phi_m - \phi_n), \quad (1)$$

$$A_{ij} = \frac{2\pi}{\Phi_0} \int_i^j \mathbf{A}^{(2)} \cdot d\mathbf{r}^{(2)}, \quad \mathbf{B} = \nabla \times \mathbf{A}, \quad (2)$$

where the magnetic field is applied along the  $c$  axis. The periodic boundary condition is applied in all directions. A columnar defect is defined as a set of four weak interactions  $J_{ij} = (1 - \epsilon)J$  surrounding a plaquette in the  $ab$  plane. Such defects distribute randomly in the  $ab$  plane with probability  $p$ , and take the same position along the  $c$  axis. Other interactions in the  $ab$  plane are given by  $J_{ij} = J$ . This modeling of columnar defects is a variant of our previous study on point defects. [14] Here we concentrate on the model with the anisotropy  $\Gamma = 5$ , the density of flux lines  $f = 1/25$ , the strength of defects  $\epsilon = 0.1$ , and the system size  $L_a = L_b = 50$  and  $L_c = 80$ . CPU time is  $1 \sim 6 \times 10^7$  Monte Carlo steps (MCS) for equilibration, and  $1 \sim 3 \times 10^7$  MCS for measurements. Since such long simulation time is required for taking equilibrium data, the present results are based on one typical configuration of columnar defects for each  $p$ .

\*Also at Lyman Lab. of Physics, Harvard University, Cambridge, MA 02138; Electronic address: nonomura.yoshihiko@nims.go.jp

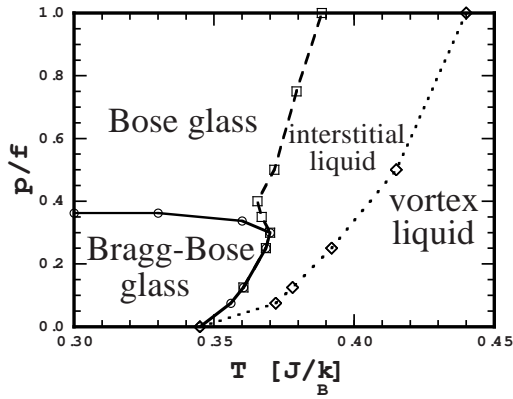


FIG. 1: Phase diagram of vortex states of high- $T_c$  superconductors with sparse and weak columnar defects in the plane of number of columnar defects per flux line versus temperature.  $p/f = 1$  corresponds to the matching field.

First, we fix the density of columnar defects for  $p = 0.01$  ( $p/f = 0.25$ ) and vary the temperature. From now on, this density is expressed in terms of the number of defects per flux line  $p/f$  with  $f = 1/25$  in order to clarify the physical situation. The specific heat  $C$  shows a sharp peak around  $T \approx 0.37J/k_B$  (marked in Fig. 2(a)), and the maximum value of the structure factor drops at the same temperature (Fig. 2(b)). These facts indicate that the melting transition occurs at  $T_m \approx 0.37J/k_B$ . The structure factor shows sharp hexagonal Bragg spots below  $T_m$  as displayed in Fig. 2(c). Coexistence of two phases is observed between  $T = 0.368J/k_B$  and  $0.374J/k_B$  owing to finite-size effects. These findings suggest that the transition at  $T_m$  is of first order. Similar results are obtained for  $p/f = 0.075, 0.125$  and  $0.30$ .

Since the helicity modulus along the  $c$  axis  $\Upsilon_c$  takes a finite value when flux lines are frozen along the  $c$  axis, the vanishing point of  $\Upsilon_c$  corresponds to the boundary between the IL and VL. As shown in Fig. 2(a), temperature dependence of this quantity changes around  $T_m$ , and it vanishes at  $T_{IL} \approx 0.392J/k_B$ , which is close to the broad peak of  $C$ . Simulations for  $p/f = 0.075, 0.125, 0.50$  and  $1.00$  show similar temperature dependence of  $\Upsilon_c$  except for monotonic increase of  $T_{IL}$  as  $p$  increases. Size dependence of  $T_m$  and  $T_{IL}$  is checked for  $p/f = 0.075$  and  $0.25$  using data with  $L_c = 54, 80$  and  $160$ , and found to be smaller than that of  $T_m$  of the pure system. [15]

As displayed in Fig. 2(b), the ratio of entangled flux lines to total flux lines  $N_{ent}/N_{flux}$  rapidly increases from  $0.3$  to  $0.5$  around  $T_m$  as in the pure system. [15] Gradual increase of  $N_{ent}/N_{flux}$  in the IL region indicates the process that untrapped flux lines are freed from trapped ones.  $N_{ent}/N_{flux} \simeq 0.85$  at  $T_{IL}$  is comparable to the value at the onset of the VL phase in the pure system. [15]

Second, we vary the density of columnar defects for  $T = 0.300J/k_B$ . As shown in Fig. 3, the maximum value of the structure factor drops at the BBG-BG phase boundary. Although anomalies of thermodynamic quan-

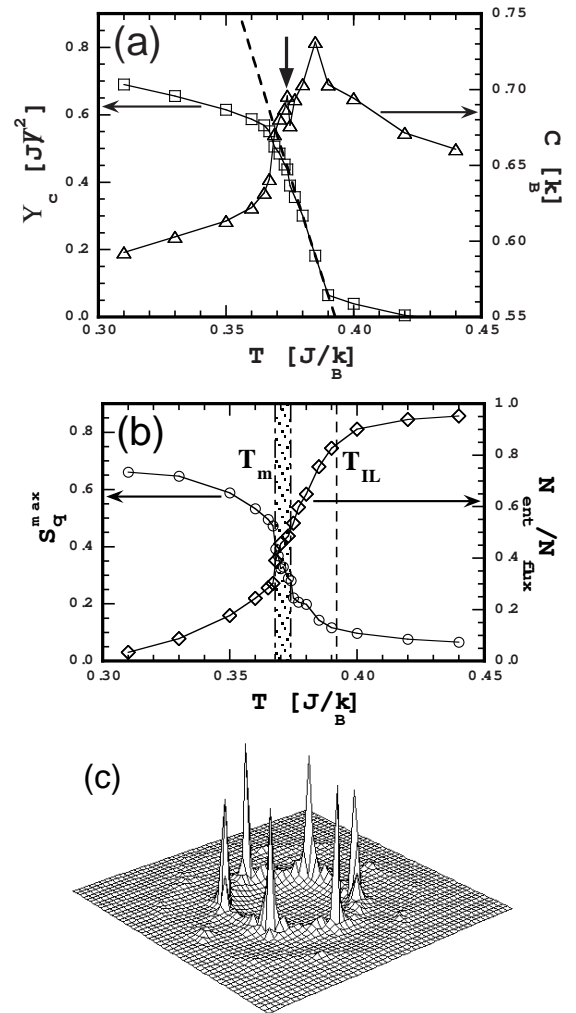


FIG. 2: Numerical results for  $p/f = 0.25$ . (a) Temperature dependence of the specific heat (triangles) and the helicity modulus along the  $c$  axis (squares). Marked is the sharp peak of the specific heat at  $T_m$ . (b) Temperature dependence of the maximum value of the structure factor (circles) and the ratio of entangled flux lines to total flux lines (diamonds). Coexistence of two phases is observed in the hatched region. (c) Structure factor at  $T = 0.36J/k_B$ .

ties such as the internal energy are too weak to observe numerically in the present study, the change of the symmetry of Bragg spots is quite apparent as depicted explicitly in Fig. 3. The hexagonal symmetry of Bragg spots at  $p/f = 0.35$  (BBG phase) is lost at  $p/f = 0.375$  (BG phase) and a glassy ring-like pattern appears. Similar results are obtained for  $T = 0.330J/k_B$  and  $0.360J/k_B$ .

Third, in order to evaluate the BG transition temperature  $T_g$ , the tilt modulus  $c_{44}$  is measured. The inverse of this quantity is proportional to the zero-field susceptibility of the transverse magnetization  $m^\perp$  of the transverse field  $H^\perp$ , namely  $c_{44}^{-1} \sim \partial \langle m^\perp \rangle / \partial H^\perp |_{H^\perp=0}$ . The Hamiltonian under the transverse field is given by  $\mathcal{H} = \mathcal{H}_0 - H^\perp m^\perp$ , where  $\mathcal{H}_0$  stands for the Hamilto-

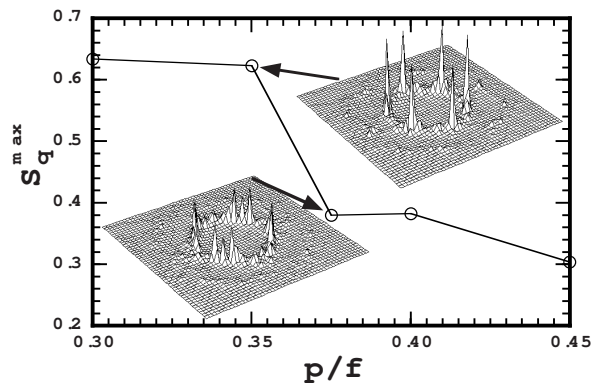


FIG. 3: Defect density dependence of the maximum value of the structure factor for  $T = 0.300J/k_B$ . Structure factors at  $p/f = 0.35$  and  $0.375$  are also displayed.

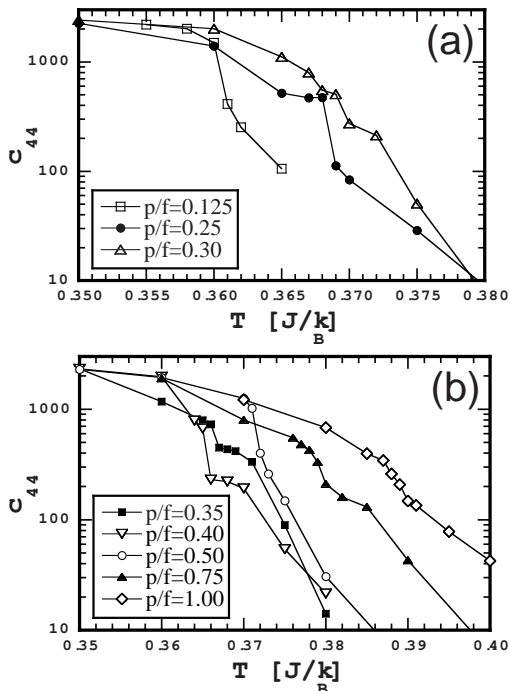


FIG. 4: Temperature dependence of the tilt modulus defined in eq. (3) for (a)  $p/f = 0.125$  to  $0.30$  and for (b)  $p/f = 0.35$  to  $1.00$ .

nian without the transverse field given in eq. (1), and the transverse magnetization  $m^\perp$  is defined from the sum of the difference of positions of flux lines along the direction of  $H^\perp$  at the top and bottom  $ab$  planes. Explicitly,  $c_{44}$  is given, aside from the coefficient, by [4]

$$c_{44} \sim \frac{N_{\text{flux}} k_B T}{\langle (m^\perp)^2 \rangle_{H^\perp=0}}. \quad (3)$$

Temperature dependence of  $c_{44}$  for  $p/f = 0.125$  to  $0.30$  (BBG-IL boundary) and for  $p/f = 0.35$  to  $1.00$  (BG-IL boundary) is displayed in Figs. 4(a) and 4(b), respec-

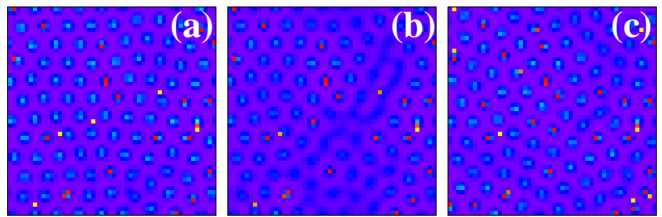


FIG. 5: Top view of averaged positions of flux lines with respect to 80 planes and 2000 independent snapshots at (a)  $p/f = 0.25$  and  $T = 0.360J/k_B$  (BBG phase), (b)  $p/f = 0.25$  and  $T = 0.380J/k_B$  (IL region), and (c)  $p/f = 0.40$  and  $T = 0.360J/k_B$  (BG phase). Columnar defects are painted in yellow (no flux lines) to red (filled with flux lines), and other regions are painted in violet (no flux lines) to light blue (largest probability of flux lines).

tively. In both cases,  $c_{44}$  shows a large jump (note that these figures are drawn in semi-log scale) at  $T_g$ . This jump is expected to be infinite in the thermodynamic limit. Since  $T_g$  coincides with  $T_m$  for  $p/f \leq 0.30$  (see Figs. 1 and 4(a)), the diverging behavior of  $c_{44}$  is observed in the whole region of the BBG phase.

Next, real-space images of flux lines are shown in Fig. 5. Positions of flux lines are averaged in all  $ab$  planes and during  $10^6$  MCS (measured for every 500 MCS). Details of these rainbow-color figures are explained in the caption. At  $p/f = 0.25$  and  $T = 0.360J/k_B$  (Fig. 5(a)), all flux lines are localized and seem to form a triangular lattice, which characterizes the BBG phase. At  $p/f = 0.25$  and  $T = 0.380J/k_B$  (Fig. 5(b)), the overall order does not exist any more, though columnar defects still trap flux lines. These properties are consistent with those of the IL region. At  $p/f = 0.40$  and  $T = 0.360J/k_B$  (Fig. 5(c)), although all flux lines are localized, the FLL structure seen in Fig. 5(a) is totally destroyed. Since most columnar defects are occupied by flux lines unless other occupied ones are nearby, many dislocations inevitably appear. These properties signal the BG phase.

Finally, interesting points of the phase diagram given in Fig. 1 are discussed. The most important feature is the existence of the BBG phase, which has not been observed experimentally or numerically until present. Giamarchi and Le Doussal [16] argued that nature of the glass order of the three-dimensional vortex states with columnar defects is equivalent to that of the two-dimensional vortex states with point defects, and pointed out [11] the possibility of the BBG phase. Stability of the quasi long-range order against topological dislocations was discussed by D. S. Fisher, [17] and he showed that this order is destroyed in  $d = 2$  but stable in  $d = 3$ . Our finding is consistent with these analytic studies.

The melting temperature  $T_m$  of the BBG phase increases as the density of columnar defects  $p$  increases up to  $p/f = 0.30$ . This behavior may look strange at a glance because the FLL order is enhanced by introducing randomness. The key to understand this exotic behavior is the real-space image of flux lines in the BBG

phase given in Fig. 5(a). There exists some unoccupied columnar defects (yellow dots) even though no occupied defects are nearby. This fact suggests that the elastic repulsion between flux lines is dominant in the BBG phase and makes the columnar defects far from stable positions of FLL remain unoccupied. Owing to this “selected pinning” mechanism, increase of  $p$  does not seriously affect energy cost for FLL distortion, but bring energy gain from pinning of flux lines by the columnar defects close to stable positions of FLL. In this case,  $T_m$  increases as  $p$  increases. As temperature increases, the BBG melts into the IL and the number of occupied flux lines increases as shown in Fig. 5(b). This behavior can also be explained naturally by the above mechanism.

When  $p$  further increases, energy gain from pinning of flux lines by many columnar defects exceeds that from FLL formation, and the transition to the BG phase takes place. The position of the BBG-BG phase boundary thus depends on the strength of columnar defects  $\epsilon$ . When  $\epsilon$  increases, this phase boundary shifts toward smaller  $p$ . Actually, simulations for  $\epsilon = 0.5$  at  $p/f = 0.25$  results in the BG phase at low temperatures, where the BBG phase exists for  $\epsilon = 0.1$  (Fig. 1). There might be a critical value  $\epsilon_c$  above which no BBG phase exists for any  $p$ .

The boundary between the BBG or BG and IL phases (on which  $c_{44}$  jumps) is not monotonic in the vicinity of the BBG-BG phase boundary. This result shows a sharp contrast to the cage-model analysis, [18] where the “melting temperature” monotonically increases as the strength of columnar defects increases. In the cage model, the system is reduced to a single flux line in a mean-field potential, and the BBG and BG phases cannot be distinguished any more. We consider that the monotonic melting line obtained from the cage model corresponds to the BG-IL phase boundary above  $p/f = 0.40$ . When this smooth curve is extrapolated to  $p = 0$ , it seems to meet the melting temperature of the pure system,  $T_m^{\text{pure}}$ . The excess superconducting region below  $p/f = 0.40$  is due to a nontrivial interplay between columnar defects and FLL structure, which is the origin of the BBG phase.

In the melting transition of FLL in pure systems, sudden entanglement of flux lines and increase of dislocations in the  $ab$  plane occur simultaneously, and dominance of these two contributions has been discussed. Random columnar defects along the  $c$  axis suppress entanglement of flux lines while enhance dislocations in the  $ab$  plane. The relation  $T_m > T_m^{\text{pure}}$  might suggest that proliferation of entanglement of flux lines rather than that of dislocations in the  $ab$  plane is the main driving force of the melting transition.

Three-dimensional vortex systems with columnar defects can be mapped to the two-dimensional interacting bosons in a random potential in the ground state. [2] Then, the present result indicates that the quasi long-range order of interacting bosons in two dimensions is stable in the presence of sparse and weak randomness.

In conclusion, the phase diagram of vortex states of high- $T_c$  superconductors with sparse and weak columnar defects is obtained by large-scale Monte Carlo simulations as shown in Fig. 1. The Bragg-Bose glass phase characterized by Bragg spots with hexagonal symmetry and the diverging tilt modulus is observed for the first time. The melting temperature to the interstitial liquid region increases as the density of columnar defects increases owing to a “selected pinning” mechanism. When the density of defects further increases, a transition to the Bose glass phase takes place. The interstitial liquid region lies between the Bragg-Bose glass or Bose glass phases and the vortex liquid phase.

The authors thank D. R. Nelson, L. Radzihovsky, B. Halperin, E. Zeldov, U. C. Täuber, L. Balents, R. Ikeda and A. Tanaka for helpful comments. Numerical calculations were performed on Numerical Materials Simulator (NEC SX-5) at Computational Materials Science Center, National Institute for Materials Science, Japan. This study is partially supported by the Priority Grant No. 14038240 from Ministry of Education, Culture, Sports, Science and Technology, Japan. One of the authors (Y. N.) was supported by the Atomic Energy Research Fund from the same Ministry.

- 
- [1] L. Civale *et al.*, Phys. Rev. Lett. **67**, 648 (1991).
  - [2] D. R. Nelson and V. M. Vinokur, Phys. Rev. Lett. **68**, 2398 (1992); Phys. Rev. B **48**, 13060 (1993).
  - [3] C. Wengel and U. C. Täuber, Phys. Rev. Lett. **78**, 4845 (1997); Phys. Rev. B **58**, 6565 (1998); and Refs. therein.
  - [4] J. Lidmar and M. Wallin, Europhys. Lett. **47**, 494 (1999); and Refs. therein.
  - [5] A. Vestergren *et al.*, cond-mat/0208225.
  - [6] L. Radzihovsky, Phys. Rev. Lett. **74**, 4923 (1995).
  - [7] P. Sen *et al.*, Phys. Rev. Lett. **86**, 4092 (2001).
  - [8] A. Nandgaonkar *et al.*, Phys. Rev. B **66**, 104527 (2002).
  - [9] T. Nattermann, Phys. Rev. Lett. **64**, 2454 (1990).
  - [10] T. Giamarchi and P. Le Doussal, Phys. Rev. Lett. **72**, 1530 (1994); Phys. Rev. B **52**, 1242 (1995).
  - [11] T. Giamarchi and P. Le Doussal, Phys. Rev. B **55**, 6577 (1997).
  - [12] Y.-H. Li and S. Teitel, Phys. Rev. B **47**, 359 (1993).
  - [13] X. Hu *et al.*, Phys. Rev. Lett. **79**, 3498 (1997); Phys. Rev. B **58**, 3438 (1998).
  - [14] Y. Nonomura and X. Hu, Physica C **341-348**, 1307 (2000); Phys. Rev. Lett. **86**, 5140 (2001).
  - [15] Y. Nonomura *et al.*, Phys. Rev. B **59**, R11 657 (1999); J. Low Temp. Phys. **147**, 1447 (1999).
  - [16] T. Giamarchi and P. Le Doussal, Phys. Rev. B **53**, 15 206 (1996).
  - [17] D. S. Fisher, Phys. Rev. Lett. **78**, 1964 (1997).
  - [18] Y. Y. Goldschmidt, Phys. Rev. B **56**, 2800 (1997).